Check for updates

Analysis of temperature-dependent dark current transport mechanism for GaAs-based blocked-impurity-band (BIB) detectors

Xiaodong Wang[1] · Yulu Chen[1] · Xiaoyao Chen[2] · Bingbing Wang[1] ·
Chuansheng Zhang[1] · Haoxing Zhang[1] · Ming Pan[1]

Abstract
Temperature-dependent dark current transport mechanism has been analyzed for GaAs-based blocked-impurity-band detectors. Device structure, processing steps and physical models are described in detail. In this work, the analysis of dark current transport mechanism has been greatly simplified by electron drift current related discussion based on the assumption that the diffusion current and the generation–recombination current as two dominating components of dark current in the absorbing layer can be equivalent to the electron drift current in the blocking layer. After confirming this assumption, our discussion focuses on why dark current is a monotonically increasing function of operation temperature for a fixed anode bias. Our results reveal that from dark current suppression point of view, low donor doping level and low operation temperature are preferred.

Keywords Gallium arsenide (GaAs) · Blocked-impurity-band (BIB) · Blocking layer ·
Operation temperature · Dark current · Electron drift current

1 Introduction

Terahertz (THz) wave lies between the microwave and infrared in the electromagnetic wave spectrum. Due to the safety, penetrability, fingerprint property, and its wide distribution, THz wave possesses substantial application values in the areas of electronics, information,

✉ Yulu Chen
  yukiylc@163.com

1 The 50th Research Institute of China Electronics Technology Group Corporation, 318 Chang He Road, Shanghai 200331, China

2 Laboratory of Advanced Material, Fudan University, Shanghai 200438, China

biology, national defense, and aerospace technology. Therefore, THz technology (Siegel 2004; Song and Nagatsuma 2011) has become one of the most important technologies so many countries and governments are willing to support and develop. For example, the US has identified THz technology as one of the most important ten technologies which can change the future of the world in 2004; Japan has established THz technology as the top priority of national key technologies in 2005.

Nowadays, THz technology research primarily focuses on THz source and THz detector. Among them, THz detector consists of Schottky diode (Liu et al. 2010), bolometer (Cherednlchenko et al. 2011), HEB (Semenov et al. 2007), SIS mixer (Shan et al. 2010), STJ detector (Ariyoshi et al. 2006), TES (Rogalski and Sizov 2011), QWIP (Liu et al. 2004), and BIB detector (Wang et al. 2016a), and the different detector corresponds to the different detection principle. For example, Schottky diode can realize THz detection by increasing microwave frequency to THz frequency; Blocked-impurity-band (BIB) detector is a novel THz detector, and its detection principle is contrary to the case of Schottky diode, the THz wave can be detected by decreasing infrared frequency to THz frequency. BIB detector has the advantages including high sensitivity, large array size, and wide response spectrum, and thus has bright application prospects in the field of air monitoring, astronomical observation, and concealed contraband detection, etc. BIB detectors can be realized based on different material systems (i.e., Si, Ge, and GaAs). Among them, Si-based BIB detector with the frequency coverage of 7.5 THz is the most widely used due to the maturity of Si material; the response frequency of Ge-based BIB can be reduced to 1.4 THz because the bonding energy of shallow impurity level in the Ge is much lower than that in Si; GaAs-based BIB detector can further reduce the response frequency to as low as 0.6 THz, and thus has the potential application in the security check and drug detection.

The key functional structure of GaAs-based BIB detector consists of a highly doped absorbing layer and an intrinsic blocking layer. Among them, the role of the absorbing layer is to excite photo-generated carriers by absorbing incident THz radiation, while the role of the blocking layer is to suppress dark current by blocking hopping current path. At present, the research and development of GaAs-based BIB detector are still on the initial stage. No GaAs-based BIB focal plane array detector has been reported all over the world due to the large dark current. For example, Reichertz et al. (2005), from UC Berkeley investigated the dependence of dark current on the bias voltage at 2.2 K, and showed the phenomenon that dark current starts to increase tremendously when the bias voltage approaches 0.63 V. However, the physical mechanism behind the phenomenon has not been explored, and thus it is still not clear how to decrease dark current and increase the array format of GaAs-based BIB detector. Besides, operation temperature as a sensitive parameter can influence the dark current of GaAs-based BIB detector to a large extent, and the different operation temperature corresponds to the different physical mechanism. Therefore, in this work, the comprehensive analysis of temperature-dependent dark current characteristics has been made to provide a good insight into the dark current transport mechanism.

2 Device structure and physical models

Cross-sectional view of GaAs-based BIB detector is shown in Fig. 1, and all the functional structures are presented in the numerical order. They are: (1) GaAs conducting substrate with donor concentration of 5×10^{18} cm^{-3}, (2) absorbing layer with donor concentration
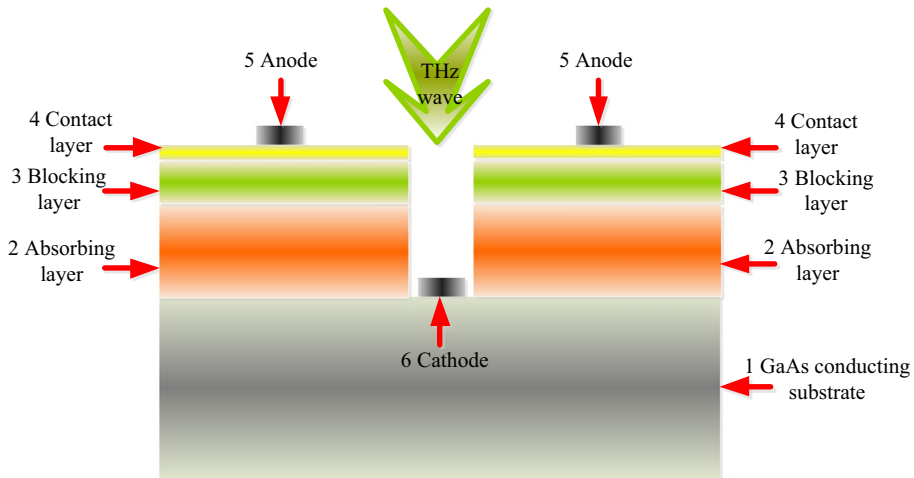
Fig. 1 Device structure of GaAs-based BIB detector

of 5×10^{15} cm^{-3}, (3) blocking layer with donor concentration of 5×10^{13} cm^{-3}, (4) contact layer with donor concentration of 3×10^{19} cm^{-3}, (5) anode, and (6) cathode, respectively. From the device processing point of view, the absorbing layer (2) and the blocking layer (3) are sequentially grown on the GaAs conducting substrate (1) in MOCVD system; the contact layer (4) are formed on the blocking layer (3) by ion implantation; the anode (5) is formed upon the contact layer (4) by electron beam evaporation; the cathode (6) is formed upon the GaAs conducting substrate (1) after deep etching to remove the contact layer (4), the blocking layer (3), and the absorbing layer (2) in the etching zone. The THz wave is front-illuminated on the device.

To analyze the temperature-dependent dark current characteristics of GaAs-based BIB detector, the drift–diffusion package (Wang et al. 2012) is used, which consists of the Poission equation, the carriers' continuity equations, and the current transport equations. Besides, the key physical models utilized by the package include generation–recombination model (Wang et al. 2014), high-field saturation model (Wang et al. 2016b), and incomplete ionization model (Wang et al. 2016c), and the above three models are all temperature dependent. Therefore, it is necessary to find a simplified way for analyzing the dark current transport mechanism. In this work, the diffusion current and the generation–recombination current as two dominating components of dark current in the absorbing layer is equivalent to the electron drift current in the blocking layer, and thus the analysis of dark current transport mechanism can be greatly simplified by electron drift current related discussion.

3 Results and discussion

Figure 2 presents dark current as a function of anode bias with operation temperature (T_O) increasing from 4 K to 30 K in 2 K steps. It is found that for a fixed T_O the relationship between dark current and anode bias can be classified into three phases: (1) dark current is independent of anode bias; (2) dark current increases rapidly with anode bias; (3) dark current increases slowly with anode bias. For phase (1), dark current fluctuates around a relatively low level corresponding to the turn-off status of dark current. For phase (2), dark

Fig. 2 Dark current as a function of anode bias for different T_O. Inset shows the relationship between V_T and T_O
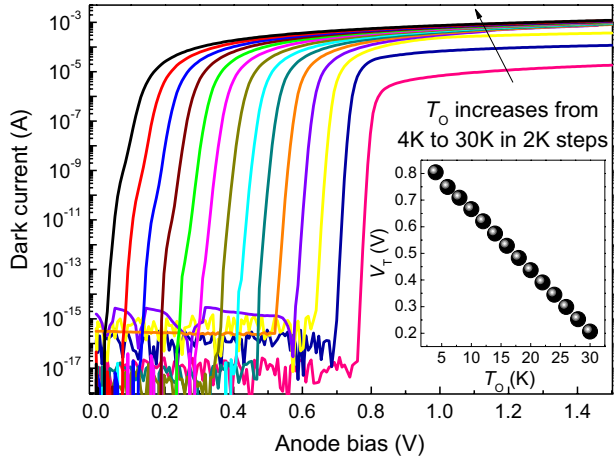
current turns on and approaches a relatively high level rapidly. For phase (3), the slope of dark current versus anode bias decreases gradually and eventually approaches a certain value. Moreover, for a fixed anode bias dark current is a monotonically increasing function of T_O. For better understanding the relationship between dark current and T_O, the lowest anode bias inducing turn-on of dark current is defined as the threshold voltage (V_T), and the linear dependence of V_T on T_O is obtained as shown in the inset of Fig. 2.

In order to explain the temperature-dependent dark current characteristics shown in Fig. 2, the dark current transport mechanism of GaAs-based BIB detector must be clarified. In our previous work (Wang et al. 2017), it has been demonstrated that the dark current in the absorbing layer is dominated by diffusion current (Hu et al. 2013, 2014) and generation–recombination current (Qiu et al. 2015, 2016). These two current components contribute dark current by providing extra carriers in both conduction band and impurity band. Specifically, the transport of extra electrons in the conduction band can give rise to the electron current, while the transport of extra vacancies in the impurity band can give rise to the hopping current. For the blocking layer, the situation is completely different. Ionized impurity and generation–recombination center can hardly be found in the blocking layer due to its high-purity property, and thus the dark current in the blocking layer is only dominated by electron drift current. Based on the principle of current continuity, the analysis of diffusion current ($I_{diffAbs}$) and generation–recombination current ($I_{g\text{-}rAbs}$) in the absorbing layer can therefore be equivalent to the discussion of electron drift current ($I_{nDriftBlo}$) in the blocking layer. As a result, the dark current of GaAs-based BIB detector (I_{dark}) can be expressed as:

$$I_{dark} = I_{diffAbs} + I_{g\text{-}rAbs} = I_{nDriftBlo} = Aq\mu_n En = Aqv_n n \qquad (1)$$

where A is the photosensitive area; q is the unit electronic charge; μ_n is the electron mobility; E is electric-field intensity; v_n is electron velocity; and n is electron density. Our following discussion will focus on drift related electron behaviors in the blocking layer.

Figure 3 presents the conduction band diagrams at 1.5 V with T_O increasing from 4 K to 10 K in 1 K steps. It is found that the degree of conduction band bending become higher and the region of conduction band bending become narrower with the increased temperature, and it is noticed that the bent conduction band is completely localized in the blocking layer when $T_O \geq 10$ K. According to the Poisson equation:

Fig. 3 Conduction band diagrams at 1.5 V for different T_O
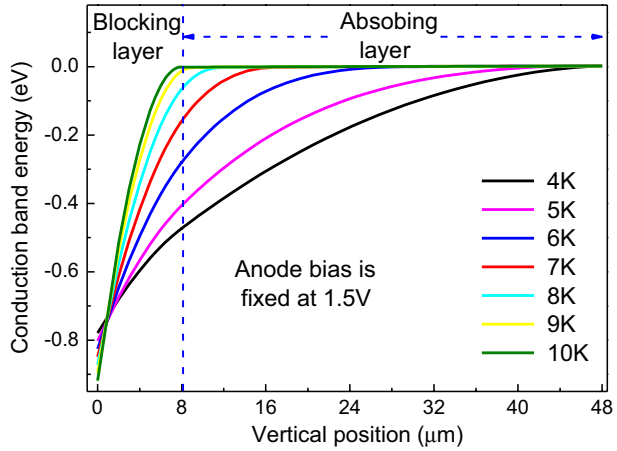
the following two equations about the electric field can be derived:

$$\frac{d^2\psi_i}{dx^2} = -\frac{\rho}{\varepsilon_s} \tag{2}$$

$$E = \frac{1}{q} \cdot \frac{dE_C}{dx} \tag{3}$$

$$\frac{dE}{dx} = -\frac{nq}{\varepsilon_s} \tag{4}$$

where ψ_i is the electrostatic potential; E_C is the bottom of the conduction band; ε_s is the dielectric constant; and x is the position along the vertical direction. The vertical distributions of electric field at 1.5 V for different T_O is presented in Fig. 4.

It is noticed that numerical simulation is completely consistent with the analytical result by comparing Fig. 4 and Eq. (3). According to Fig. 4 and Eq. (4), it can be found that a

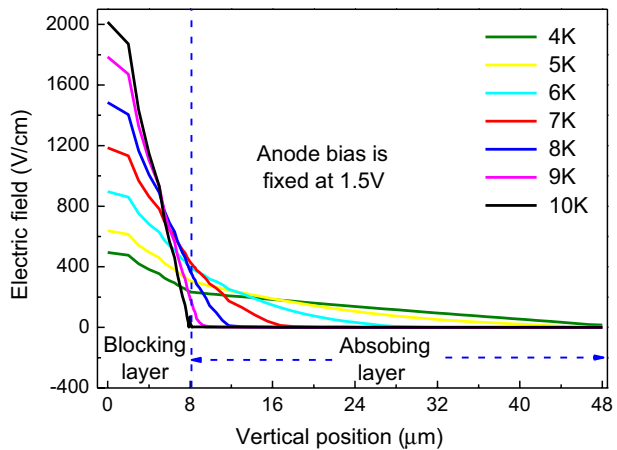**Fig. 4** Vertical distributions of electric field at 1.5 V for different T_O

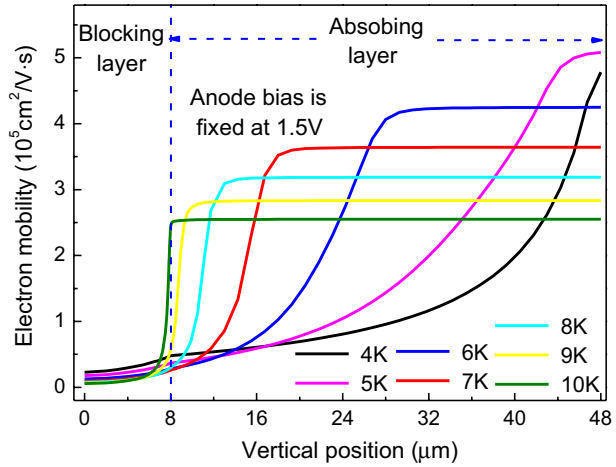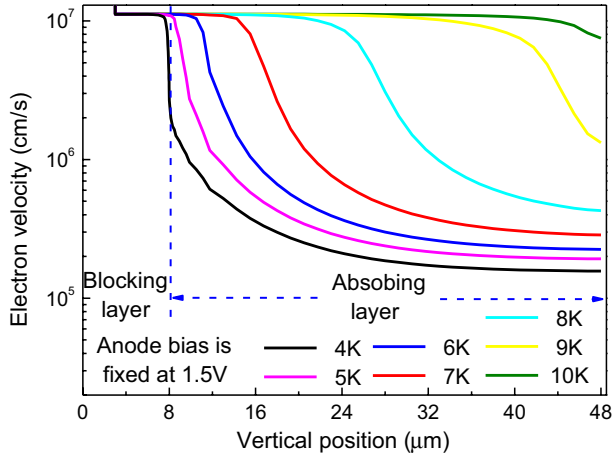**Fig. 5** Vertical profiles of electron mobility at 1.5 V for different T_O

Fig. 6 Vertical profiles of electron velocity at 1.5 V for different T_O

certain amount of negative charges accumulated in both the blocking layer and the absorbing layer. However, negative charges in the blocking layer are originated from the extra electrons transporting from the absorbing layer, while negative charges in the absorbing layer are originated from the ionized acceptors unintentionally introduced during the epitaxy process.

Figure 5 shows the vertical profiles of electron mobility at 1.5 V for different T_O. It is interesting to note that the electron mobility at $x=0$ is a monotonically decreasing function of T_O due to electron velocity saturation at such position, which can be confirmed by Fig. 6. Specifically, electron mobility (μ_n), electric field (E) and electron velocity (v_n) at $x=0$ exhibit the following relationship:

$$\mu_n E = v_n = v_{nSat} = \text{constant} \tag{5}$$

and thus Eq. (5) reduces to:

$$\mu_n \propto 1/E \tag{6}$$

Fig. 7 Vertical distributions of electron density at 1.5 V for different T_O
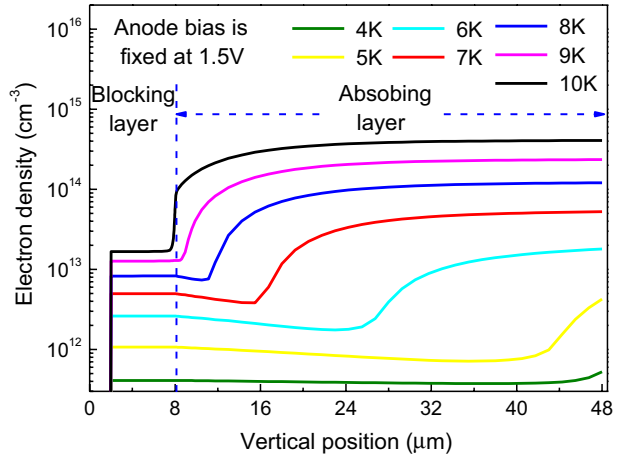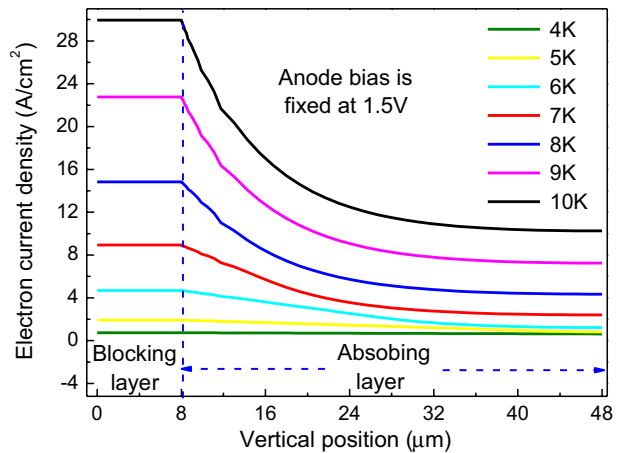

Fig. 8 Vertical profiles of electron current density at 1.5 V for different T_O

According to Fig. 4, electric field at $x=0$ is a monotonically increasing function of T_O, and thus effect of T_O on μ_n at $x=0$ is completely opposite to that on E.

Figure 7 shows the vertical distributions of electron density at 1.5 V for different T_O. It is demonstrated that a higher T_O will result in a larger electron density for both blocking and absorbing layers. Additionally, a nearly uniform distribution of electron density in the blocking layer can be observed indicating that neither diffusion nor generation–recombination process occurs; instead drift process dominates in the blocking layer, which further confirms the assumption put forward at the beginning of our discussion.

Figures 8, 9, and 10 show the vertical profiles of electron current density, hopping current density, and total current density, respectively. Comparing Figs. 8 and 9, it is interesting to note that electron current density is a monotonically increasing function of T_O, while hopping current density in the blocking layer is near zero regardless of T_O, confirming dark current in the blocking layer is dominated by electron current, instead of hopping current. On the contrary, dark current in the absorbing layer is simultaneously dominated by electron current and hopping current and the importance of hoping current become more and more prominent

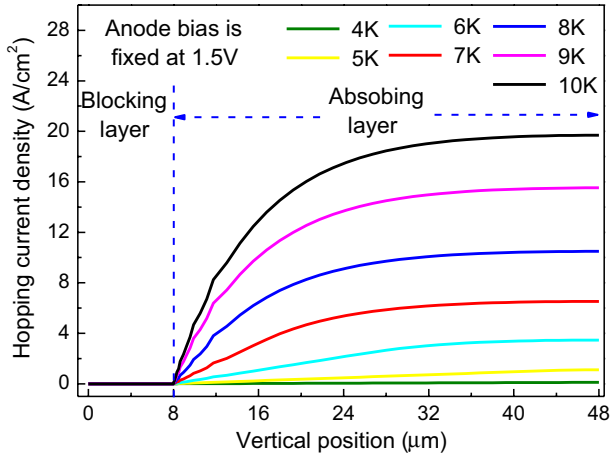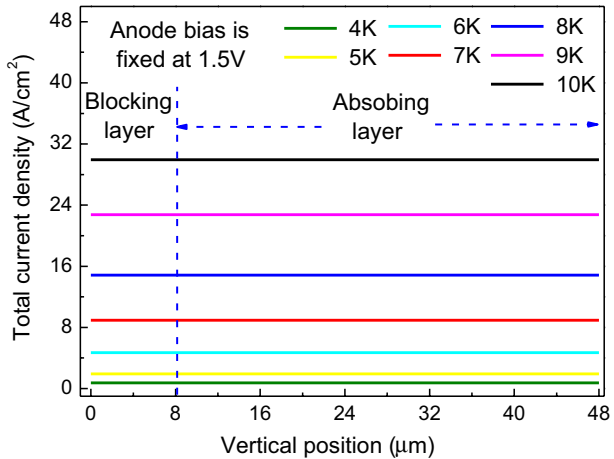**Fig. 9** Vertical profiles of hopping current density at 1.5 V for different T_O

Fig. 10 Vertical profiles of total current density at 1.5 V for different T_O

with increasing T_O. Figure 10 shows the vertical profiles of total current density at 1.5 V for different T_O. According to Fig. 10, the total current density keeps constant in either blocking layer or absorbing layer for a fixed T_O, which confirms that the analysis of electron current and hopping current in the absorbing layer can be equivalent to the discussion of electron current in the blocking layer.

Based on the above discussion, it can be concluded that the dark current in the blocking layer is dominated by electron drift current. With the increased operation temperature electron drift velocity keeps constant, while electron density monotonically increases, which can well explain why dark current is a monotonically increasing function of T_O for a fixed anode bias. The results imply that from dark current suppression point of view, low donor doping level and low operation temperature are preferred.

4 Conclusion

In this work, temperature-dependent dark current transport mechanism has been analyzed for GaAs-based blocked-impurity-band (BIB) detectors. The analysis of dark current transport mechanism can be greatly simplified by electron drift current related discussion based on the assumption that the diffusion current and the generation–recombination current as two dominating components of dark current in the absorbing layer is equivalent to the electron drift current in the blocking layer. The reason why dark current is a monotonically increasing function of operation temperature for a fixed anode bias is because electron drift velocity keeps constant, while electron density monotonically increases with the increased operation temperature. Our results reveal that from dark current suppression point of view, low donor doping level and low operation temperature are preferred.

References

Ariyoshi, S., Otani, C., Dobroiu, A., Sato, H., Kawase, K., Shimizu, H.M., Taino, T., Matsuo, H.: Terahertz imaging with a direct detector based on superconducting tunnel junctions. Appl. Phys. Lett. **20**, 203503 (2006)

Cherednlchenko, S., Hammar, A., Bevilacqua, S., Darkinskiy, V., Stake, J., Kalabukhov, A.: A room temperature bolometer for terahertz coherent and incoherent detection. IEEE Trans. Terahertz Sci. Technol. **1**, 395–402 (2011)

Hu, W.D., Chen, X.S., Ye, Z.H., Feng, A.L., Yin, F., Zhang, B., Liao, L., Lu, W.: Dependence of ion-implant-induced LBIC novel characteristics on excitation intensity for long-wavelength HgCdTe-based photovoltaic infrared detector pixel arrays. IEEE J. Sel. Topics Quantum Electron. **19**, 4100107 (2013)

Hu, W., Ye, Z., Liao, L., Chen, H., Chen, L., Ding, R., He, L., Chen, X., Lu, W.: A 128×128 longwavelength/mid-wavelength two-color HgCdTe infrared focal plane array detector with ultra-low spectral crosstalk. Opt. Lett. **39**, 5130–5133 (2014)

Liu, H.C., Song, C.Y., SpringThorpe, A.J., Cao, J.C.: Terahertz quantum-well photodetector. Appl. Phys. Lett. **84**, 4068–4070 (2004)

Liu, L., Hesler, J.L., Xu, H., Lichtenberger, A.W., Weikle II, R.M.: A broadband quasi-optical terahertz detector utilizing a zero bias schottky diode. IEEE Microw. Wirel. Compon. Lett. **20**, 504–506 (2010)

Qiu, W.C., Hu, W.D., Chen, L., Lin, C., Cheng, X.A., Chen, X.S., Lu, W.: Dark current transport and avalanche mechanism in HgCdTe electron-avalanche photodiodes. IEEE Trans. Electron Devices **62**, 1926–1931 (2015)

Qiu, W.C., Hu, W.D., Lin, C., Chen, X.S., Lu, W.: Surface leakage current in 12.5 μm long-wavelength HgCdTe infrared photodiode arrays. Opt. Lett. **41**, 828–831 (2016)

Reichertz, L.A., Cardozo, B.L., Beeman, J.W., Larsen, D.I., Tschanz, S., Jakob, G., Katterloher, R., Haegel, N.M., Haller, E.E.: First results on GaAs blocked impurity band (BIB) structures for far-infrared detector arrays. Proc. SPIE **5883**, 58830Q (2005)

Rogalski, A., Sizov, F.: Terahertz detectors and focal plane arrays. Opto-Electron. Rev. **19**, 346–404 (2011)

Semenov, A.D., Richter, H., Huebers, H.W., Gunther, B., Smirnov, A., Ilin, K.S., Siegel, M., Karamarkovic, J.P.: Terahertz performance of integrated lens antennas with hot-electron bolometer. IEEE Trans. Microw. Theory Tech. **55**, 239–247 (2007)

Shan, M.L., Takeda, M., Kojima, T., Uzawa, Y., Shi, S.C., Noguchi, T., Wang, Z.: Low-noise waveguide-type NbN/AlN/NbN SIS mixers approaching terahertz frequencies. IEEE Trans. Microw. Theory Tech. **58**, 841–843 (2010)

Siegel, P.H.: Terahertz technology in biology and medicine. IEEE Trans. Microw. Theory Tech. **52**, 2438–2447 (2004)

Song, H.J., Nagatsuma, T.: Present and future of terahertz communications. IEEE Trans. Terahertz Sci. Technol. **1**, 256–263 (2011)

Wang, X.D., Hu, W.D., Chen, X.S., Lu, W.: The study of self-heating and hot-electron effects for AlGaN/GaN double-channel HEMTs. IEEE Trans. Electron Devices **59**, 1393–1401 (2012)

Wang, X.D., Hu, W.D., Pan, M., Hou, L.W., Xie, W., Xu, J.T., Li, X.Y., Chen, X.S., Lu, W.: Study of gain and photoresponse characteristics for back-illuminated separate absorption and multiplication GaN avalanche photodiodes. J. Appl. Phys. **115**, 013103 (2014)

Wang, X., Wang, B., Hou, L., Xie, W., Chen, X., Pan, M.: Analysis of dark current and spectral response mechanisms for Si-based block-impurity-band detectors operating at terahertz regime. Opt. Quantum Electron. **48**, 100 (2016a)

Wang, X., Wang, B., Chen, X., Chen, Y., Hou, L., Xie, W., Pan, M.: Roles of blocking layer and anode bias in processes of impurity-band transition and transport for GaAs-based blocked-impurity-band detectors. Infrared Phys. Technol. **79**, 165–170 (2016b)

Wang, X., Wang, B., Chen, Y., Hou, L., Xie, W., Chen, X., Pan, M.: Spectral response characteristics of novel ion-implanted planar GaAs blocked-impurity-band detectors in the terahertz domain. Opt. Quantum Electron. **48**, 518 (2016c)

Wang, X., Chen, Y., Chen, X., Wang, B., Zhang, C., Zhang, H., Pan, M.: Dark current transport mechanism associated with acceptor concentration in GaAs-based blocked-impurity-band (BIB) detectors. Opt. Quantum Electron. **49**, 419 (2017)